



HAL
open science

Numerical and experimental investigation on topology optimization of an elongated dynamic system

Heitor Nigro Lopes, D.C. Cunha, R. Pavanello, Jarir Mahfoud

► **To cite this version:**

Heitor Nigro Lopes, D.C. Cunha, R. Pavanello, Jarir Mahfoud. Numerical and experimental investigation on topology optimization of an elongated dynamic system. *Mechanical Systems and Signal Processing*, 2022, 165, 10.1016/j.ymssp.2021.108356 . hal-03659789

HAL Id: hal-03659789

<https://hal.science/hal-03659789>

Submitted on 21 Nov 2023

HAL is a multi-disciplinary open access archive for the deposit and dissemination of scientific research documents, whether they are published or not. The documents may come from teaching and research institutions in France or abroad, or from public or private research centers.

L'archive ouverte pluridisciplinaire **HAL**, est destinée au dépôt et à la diffusion de documents scientifiques de niveau recherche, publiés ou non, émanant des établissements d'enseignement et de recherche français ou étrangers, des laboratoires publics ou privés.

Numerical and experimental investigation on topology optimization of an elongated dynamic system

Heitor Nigro Lopes ^{a,*}, Daniel Candeloro Cunha ^a, Renato Pavanello ^a, Jarir Mahfoud ^b

a Department of Computational Mechanics, School of Mechanical Engineering, University of Campinas, Rua Mendelejev 200, 13083-860 Campinas, Brazil

b University of Lyon, INSA-Lyon, CNRS UMR5259, LaMCoS, Villeurbanne F-69621, France

Minimizing vibration levels of dynamic components at their operating frequency range has been a widely studied topic in engineering. However, the design of structures that satisfy geometric constraints and technical performances is an ongoing challenge. In this work, a topology optimization procedure based on the Bi-directional Evolutionary Structural Optimization (BESO) algorithm is performed to maximize the natural frequency separation interval of an elongated structure. The issues of disconnected and trivial solutions are solved using a connectivity constraint. It is imposed by a proposed procedure based on the heat flux solution of an auxiliary system. An assessment of the feasibility of the structure is done by verifying its accordance with manufacturing and design constraints. The optimized structure was manufactured and validated experimentally. The implemented process produces topologies that maximize the natural frequency separation and reduce the mass of the structure. The obtained results demonstrate the effectiveness of the proposed procedure at satisfying geometric design constraints and technical performances.

1. Introduction

In engineering problems, excessive vibration is usually associated with undesirable consequences, such as failure. Usually, for rotating systems, operating frequencies are chosen far from resonance speeds. In some applications, it is not easy to maintain a constant speed, especially when undergoing variable loads. For this reason, it is advantageous to ensure a large enough separation margin between the operating frequency and the nearby resonance frequencies. Therefore, controlling the natural frequencies of a structure is the objective of many optimization applications [1].

The topology optimization method is a well-established method for structural optimization. First introduced by Bendsøe and Kikuchi [2] as a shape optimization algorithm based on the homogenization method, this procedure promptly started a new branch in structural optimization. The need for the homogenization method was removed after the introduction of continuous relaxation functions and penalization when defining the properties of the structure. This yielded the well-established Solid Isotropic Material with Penalization (SIMP) method [3–5]. The topology optimization method was then extended to a discrete form as the Evolutionary Structural Optimization (ESO) [6]. Its main advantage is the absence of elements with intermediary properties, which carry no physical meaning. Then, the Bi-directional Evolutionary Structural Optimization (BESO) method was proposed as an alternative to allow both the addition and removal of elements [7].

* Corresponding author.

E-mail address: lopes@fem.unicamp.br (H.N. Lopes).

These algorithms require additional procedures to avoid usual problems related to dynamic system optimization. A numerical filter is needed to avoid mesh-dependent topologies and checkerboard patterns [8,9]. Additionally, as demonstrated by Pedersen [10], the SIMP interpolation scheme results in non-physical topologies due to the dynamic behavior of void elements. A new interpolation scheme was then proposed to avoid such problem, which was subsequently adapted for the BESO [11]. With these adjustments, topology optimization algorithms proved to be robust enough for several problems. Among others, it has been implemented for fluid–structure interaction [12,13], multiscale analyses [14,15], design of piezoelectric harvesters [16] and acoustic insulators [17].

When optimizing dynamic systems, one can desire either to increase or to reduce vibration. When working with energy harvesting, clustering the natural frequencies of a system can be beneficial, because it increases the performance of the harvester [18]. When dealing with dangerous resonances, however, the separation of natural frequencies is desired. The maximization of this separation is also beneficial on the design of controllable structures [19].

In the context of topology optimization for reducing vibration of dynamic systems, there are two main alternatives: either the natural frequencies or the frequency response is optimized. Ma et al. [20,21] performed a topology optimization process based on the homogenization method to solve both types of problems. Xie and Steven [22] implemented a simple natural frequency optimization algorithm using the ESO, which was then extended to the BESO [11]. Jensen and Pedersen [23] maximized the separation interval between adjacent natural frequencies for 1D and 2D scalar cases. Du and Olhoff [24] proposed a robust algorithm for several different cases of natural frequency optimization. Two common problems in these algorithms are mode shifting and local modes. Li et al. [25] performed the optimization of dynamic responses using the Level-set method to eliminate local modes. Li et al. [26] and Lopes et al. [27] proposed methods for the optimization of natural frequency separation interval that solve both problems.

For dynamic response optimization, damping could be considered using the proportional damping model or other models with diagonal modal damping matrix [28]. These models have been used in the context of topology optimization [29], but it is important to emphasize that, even in non-diagonal damping systems, an approximated proportional one can be built [30].

In recent years, additive manufacturing has gained popularity. Despite the many challenges for successful integration of topology optimization procedures and additive manufacturing, they are powerful tools for designing and prototyping. Ma et al. [31] utilized a topology optimization procedure to maximize natural frequencies of a structure, which was subsequently manufactured and tested experimentally. To impose certain restrictions on the optimal design, a multidomain topology optimization technique was employed, calibrated by the user.

For structures with high geometric aspect ratio, such as bridges, aircraft and missiles, topology optimization procedures for natural frequencies often fail. This is due either to local optima occurring for disconnected topologies or to the presence of a trivial solution, such as reducing the length of the structure. One way to avoid this problem is to include a non-structural mass on set locations, guaranteeing their connectivity [32]. Another alternative is the addition of a compliance term in the objective function [33]. Munk et al. [34] proposed an elegant alternative, via the implementation of a connectivity filter. However, while this solution solved the connectivity problem, it lead to mesh-dependent topologies. Liu et al. [35] proposed the Virtual Temperature Method (VTM) to avoid enclosed void regions, which may lead to manufacturing difficulties. This method was recently extended to the Nonlinear Virtual Temperature Method (N-VTM) [36], which was employed to satisfy overhang angle constraints.

This work performs the topology optimization design of a structure through the following the steps: optimization, simulation and experimental validation. The main challenges of each step are assessed. First, the structure is optimized based on a frequency separation criterion. A novel connectivity approach that uses energy balance properties, similarly to the VTM, is proposed to satisfy geometric design constraints. Then, a close examination on the optimization hypotheses is done by simulating the obtained solution in a three-dimensional analysis. Finally, an experimental test is performed to validate the proposed procedures. This structure is produced via additive manufacturing and tested using a sweep harmonic excitation and measuring the displacements with a laser Doppler vibrometer. Results show correspondence between both the experimental and simulated results. The developed procedures enable a satisfactory increase of the initial frequency separation margin.

2. Procedure for structure design

In this section, the optimization problem is presented and the connectivity constraint is formulated. The algorithm for the topology optimization procedure using the BESO method is also presented.

2.1. Frequency separation interval maximization

The maximization of natural frequency separation interval of elastic structures is considered in this section. As the present problem concerns the optimization of natural frequencies, the system is modeled as undamped. This hypothesis is not too restrictive, since the damped natural frequencies and resonance frequencies change little for systems with small structural damping.

The undamped linear dynamic system can be represented by the following eigenproblem:

$$-\mathbf{M}\omega_j^2\phi_j + \mathbf{K}\phi_j = 0 \quad (1)$$

where ω_j and ϕ_j are the j th eigenvalue and eigenvector of the system. The matrices \mathbf{M} and \mathbf{K} are the global mass and stiffness matrices, obtained via the Finite Element Method. The system is assumed to be linear elastic isotropic, under the two-dimensional plane stress hypothesis, that is, the stress tensor components outside the studied plane are negligible.

In this work, the optimization goal is obtaining a structure that maximizes the natural frequency separation interval around a given operating frequency. This is done by finding the optimal material distribution along the domain. The corresponding optimization problem [21] is stated as:

$$\begin{aligned} \max \quad & f(x_i) = \omega_0^2 + \left[\sum_{j=1}^{n_m} \frac{1}{(\omega_j^2 - \omega_0^2)^2} \right]^{-1/2} \\ \text{s.t.} \quad & V^* - \sum_{i=1}^N V_i x_i = 0 \\ & x_i = 1 \text{ or } x_{\min} \end{aligned} \quad (2)$$

where ω_0 is the operating frequency around which the frequency separation interval is maximized. The parameter n_m is the number of considered eigenvalues. Its choice process consists in finding a value large enough so that the highest eigenvalues influence little on the optimization process. However, the computational cost of the optimization procedure increases proportionally to n_m , and, therefore, it must be properly adjusted by the user. In this work, this is done by choosing a value so that at least half of the n_m natural frequencies are greater than ω_0 . The design variable x_i represents the current configuration of the i th finite element, which can be either 1, for a solid element, or x_{\min} , for a void one. V^* is the imposed final volume and V_i is the volume of the i th element.

Compared to directly maximizing the difference between adjacent eigenvalues, this function has the advantage of avoiding both mode-shift and close eigenvalues problems. It is more robust to the emergence of local modes and instabilities along the process. Additionally, it can be implemented with mode tracking procedures [27].

Having defined the objective function, the sensitivity analysis is performed via the differentiation of $f(x_i)$:

$$\alpha_i = \left[\sum_{j=1}^{n_m} \frac{1}{(\omega_j^2 - \omega_0^2)^2} \right]^{-3/2} \sum_{j=1}^{n_m} \frac{1}{(\omega_j^2 - \omega_0^2)^3} \left[\phi_j^T \left(\frac{\partial \mathbf{K}}{\partial x_i} - \omega_j^2 \frac{\partial \mathbf{M}}{\partial x_i} \right) \phi_j \right] \quad (3)$$

where the eigenvectors ϕ_j are normalized with respect to the mass matrix \mathbf{M} .

The derivatives of the mass and stiffness matrices are obtained from the interpolation schemes of the density and Young's Modulus:

$$\rho(x_i) = x_i \rho_0 \quad (4)$$

$$E(x_i) = \left[\frac{x_{\min} - x_{\min}^p}{1 - x_{\min}^p} (1 - x_i^p) + x_i^p \right] E_0 \quad (5)$$

where ρ_0 and E_0 are the density and Young's modulus of the base material.

This interpolation scheme is used to avoid local modes in void elements [11]. In continuous methods, the penalization exponent p is usually defined based on the Hashin-Shtrikmann bounds [37]. In the BESO, a calibration must be done by the user, testing several different values and analyzing the evolution and the final topology. Usual values for p are around 3 [9].

The derivatives of the finite element matrices are:

$$\frac{\partial \mathbf{M}}{\partial x_i} = \mathbf{M}_0 \quad (6)$$

$$\frac{\partial \mathbf{K}}{\partial x_i} = \frac{1 - x_{\min}}{1 - x_{\min}^p} p x_i^{p-1} \mathbf{K}_0 \quad (7)$$

where \mathbf{M}_0 and \mathbf{K}_0 are the mass and stiffness matrices of a solid element.

This sensitivity analysis is necessary for the update procedure of the BESO algorithm, which will be presented in Section 2.3.

2.2. Connectivity constraint for elongated structures

Optimization problems can have trivial, degenerated solutions. The maximization of the objective function given in Eq. (2) may present such an issue, as there are cases where the optimal topologies correspond to disconnected structures, that is, structures in which regions of the design domain become disconnected.

In this work, a novel method for measuring and imposing connectivity between two given regions is developed. At each iteration, solid elements that are essential to maintain a minimal structural connectivity are identified. These elements are prevented from turning into void elements during the update procedure of the BESO.

A heat conduction equation is used to measure the importance of each element in keeping the given regions connected. The following are considered: only solid elements are thermally conductive, and a unitary heat transfer rate enters the domain through a surface Γ_a and leaves through a surface Γ_b . Under these conditions, the heat flux will be greater in thin connections between Γ_a and Γ_b . As a consequence, the heat flux passing through a solid element can be used to measure its importance in keeping both

surfaces connected. In order to compute the heat flux, an auxiliary Finite Element Analysis is performed to solve the following equation:

$$\begin{aligned}
\nabla \cdot (k(s)\nabla T(s)) &= 0 & , & \quad s \in \Omega \\
\nabla T(s) \cdot \mathbf{n}(s) &= 0 & , & \quad s \in \Gamma_o \\
k(s)\nabla T(s) \cdot \mathbf{n}(s) &= -q_a & , & \quad s \in \Gamma_a \\
k(s)\nabla T(s) \cdot \mathbf{n}(s) &= -q_b & , & \quad s \in \Gamma_b \\
T(s) &= 0 & , & \quad s \in \{s_0\}
\end{aligned} \tag{8}$$

where $T(s)$ represents the temperature field in a spatial point s ; $\mathbf{n}(s)$ represents the unit normal vector, orthogonal to the boundary surfaces and pointing outward; q_a and q_b represent the imposed fluxes. The conductivity $k(s)$ is adopted as 1 for solid elements and x_{\min} for void ones, ensuring that the heat flux passes only through solid elements. The domain Ω is the optimization domain; the surfaces Γ_a and Γ_b are the regions that must be connected; the adiabatic boundary Γ_o comprises any other boundary point; s_0 can be any point of Ω , it serves only to make the problem well-posed. ∇ is the gradient operator.

Since a unitary heat transfer rate is considered, q_a and q_b must satisfy the conditions:

$$\int_{\Gamma_a} q_a dA = -1 \tag{9}$$

$$\int_{\Gamma_b} q_b dA = 1 \tag{10}$$

Once the scalar field $T(s)$ is obtained, the vector field $\mathbf{q}(s)$ can be calculated as:

$$\mathbf{q}(s) = -k(s)\nabla T(s) \tag{11}$$

Finally, the value $q_i = \|\mathbf{q}\|$, evaluated at the center of the i th element, is used as a measure of its importance in keeping connectivity. By defining a maximal value q_{\max} , elements with $q_i \geq q_{\max}$ are excluded from the update procedure.

The parameter q_{\max} can be obtained by specifying a minimal surface area, A_{\min} , connecting Γ_a and Γ_b . Assuming that $\mathbf{q}(s)$ is uniform and orthogonal to the minimal connecting surface, q_{\max} is given by:

$$q_{\max} = \frac{1}{A_{\min}} \tag{12}$$

The essential elements are taken out from the design domain by setting their sensitivity values to the maximal value obtained in the current optimization iteration. This procedure is given by:

$$\alpha_i^c = \alpha_i + c(q_i) [\max(\alpha) - \alpha_i] \tag{13}$$

where α^c is the modified sensitivity vector, which is employed to update the topology, and $c(q_i)$ is an activation parameter.

To define a soft-activation, a minimal threshold must be considered. By specifying a reference surface area A_{\max} connecting Γ_a and Γ_b , q_{\min} is defined by:

$$q_{\min} = \frac{1}{A_{\max}} \tag{14}$$

Thus, the function $c(q_i)$ can be defined as a linear soft-activation:

$$c(q_i) = \begin{cases} 0 & , q_i \leq q_{\min} \\ \frac{q_i - q_{\min}}{q_{\max} - q_{\min}} & , q_i \in (q_{\min}, q_{\max}) \\ 1 & , q_i \geq q_{\max} \end{cases} \tag{15}$$

In this work, the imposed boundary fluxes q_a and q_b are set as uniform through Γ_a and Γ_b . Since bi-dimensional structures under plane stress hypothesis are considered, the area parameters correspond to length parameters. A_{\max} is set to be the height of the rectangular design domain, and A_{\min} is defined based on the problem specifications. The connectivity constraint imposes that the left and right extremities of the design domain are kept connected.

Fig. 1 illustrates the flux $\mathbf{q}(s)$ passing through the structure. The activation function is low in the low flux region, represented with blue arrows. In this part of the structure, the topology optimization is performed with little influence of the connectivity constraint. The activation function is high in the high flux region, represented with red arrows. In this part of the structure, topology changes are limited by the connectivity constraint.

2.3. Topology optimization method

The topology optimization method is based on finding the design that maximizes the desired criterion via successive changes to the topology. To each element, a design variable is assigned. As the BESO is a discrete procedure, these design variables can only assume discrete values, meaning that elements can only be either solid ($x_i = 1$) or void ($x_i = x_{\min}$). Void elements are considered as really flexible, instead of absent, to avoid numerical problems along the process. These design variables are updated at each iteration based on a sensitivity analysis, where the influence of each element on the objective function is evaluated.

The BESO is a well-established algorithm for topology optimization and was chosen due to its simplicity and robustness. The BESO is a gradient-based optimization procedure, meaning the sensitivity analysis is done based on the derivative of the objective

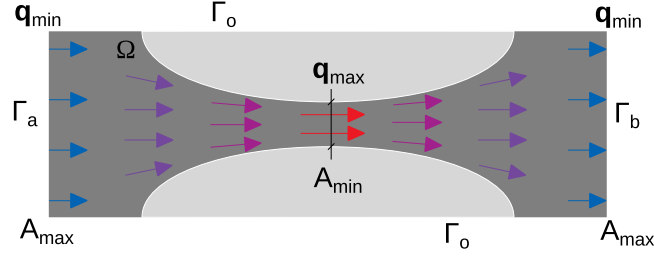


Fig. 1. Connectivity constraint soft-activation.

function, as previously presented in Eq. (3). Despite having no convergence guarantees, the BESO proved to be a powerful method for topology optimization. When used properly, it usually leads to local minima and produces feasible topologies at each iteration. The BESO procedure is shown in Algorithm 1.

Algorithm 1: BESO procedure

Input: Define parameters: x_{\min} , p , ER , AR_{\max} , V^* , r_{\min} , A_{\min} , τ , N , n_m

Define boundary conditions and mesh

Start iteration counter: $k = 0$

Calculate eigenvalues and eigenvectors

while $error < \tau$ **or** $V^{(k)} \neq V^*$ **do**

$k = k + 1$

 Evaluate sensitivities $\alpha_i^{(k)}$ (Eq. (3))

 Filter sensitivity numbers (Eqs. (16) and (17))

 Perform connectivity procedure (Eq. (13))

 Update topology $x_i^{(k)}$

 Update volume $V^{(k)}$

 Calculate eigenvalues and eigenvectors

$$error = \frac{\sum_{\sigma=k-2N}^{k-N} f(x_i^{(\sigma)}) - \sum_{\sigma=k-N}^k f(x_i^{(\sigma)})}{\sum_{\sigma=k-N}^k f(x_i^{(\sigma)})}$$

end

Output: Optimized topology $x_i^{(k)}$

In Algorithm 1, the parameters defined at the “Input” field must be given by the user. ER is the Evolutionary Rate, which corresponds to the rate of change in the volume for each iteration, and AR_{\max} is the maximum Addition Ratio, indicating the maximum percentage of element addition at a given iteration. Both parameters must be calibrated by the user. Higher values of ER and AR_{\max} may reduce the number of iterations required, but they can also destabilize the procedure. Thus, they must remain low enough to ensure a stable and coherent evolution. The parameter V^* is the final volume imposed by the design constraints.

The stopping criterion is based on the historical average and calculated via the expression shown in Algorithm 1. The parameters τ and N represent, respectively, the tolerance and the number of previous iterations considered in the averaging process.

The filtering scheme is implemented as presented by Huang and Xie [9]. It is required to avoid both checkerboard patterns and mesh-dependent solutions. The former is a numerical problem originating from the bilinear finite elements, the latter must be avoided to prevent exceedingly thin components in the optimized structure, which hinder manufacturability. It requires defining a parameter r_{\min} , which is usually interpreted as the minimum admissible thickness of the topology. Its application is based on performing two successive transforms on the sensitivity. Initially, a nodal sensitivity α_j is defined by averaging the elemental sensitivity to its nodes:

$$\alpha_j = \sum_{i=1}^M \frac{1}{M-1} \left(1 - \frac{r_{ij}}{\sum_{i=1}^M r_{ij}} \right) \alpha_i \quad (16)$$

where M is the number of elements that have the node j . The value r_{ij} is the distance between the center of the i th element and the j th node, and α_i is the elemental sensitivity calculated in Eq. (3). If M is equal to 1, then α_j is defined as equal to α_i .

These nodal sensitivities are then averaged back to the elements, weighted by the distance between the center of the elements and the nodes:

$$\alpha_i = \frac{\sum_{j=1}^P \max(0, r_{\min} - r_{ij}) \alpha_j}{\sum_{j=1}^P \max(0, r_{\min} - r_{ij})} \quad (17)$$



Fig. 2. Optimization domain.

Table 1

Optimization parameters.

Parameter	Value
AR_{\max}	2%
ER	2%
r_{\min}	2 mm
x_{\min}	10^{-6}
p	5
A_{\min}	4 mm
V^*	60%
τ	0.1%
N	5
n_m	10



Fig. 3. Optimal topology of the preliminary result.

where P is the total number of nodes.

3. Optimization results

This section presents the first part of the design, aiming at adjusting the optimization procedures for the studied structure. During this step, the system is optimized and initial assessments on its manufacturability are done. The heat flux connectivity constraint is used to that end.

The studied domain is an elongated cantilever beam, as shown in Fig. 2.

This structure is modeled using the properties of the Polylactic acid (PLA), the polymer that will be used during the experimental analysis. Its mechanical properties are: $E = 3.5$ GPa, $\nu = 0.36$ and $\rho = 1250$ kg/m³. The other optimization parameters are shown in Table 1.

The operating frequency is set to $f_0 = \omega_0/2\pi = 400$ Hz. As such, the optimization procedure is performed to increase the frequency range free of resonance around it.

3.1. Preliminary results

As stated in Section 2.2, to apply the connectivity constraint, an input and an output surfaces must be defined. The proposed ones are shown in Fig. 2, corresponding to an inflow on the left extremity and an outflow on the right one.

With the previously defined parameters, the optimization procedure is performed. After 40 iterations, the stop criteria from Algorithm 1 are met, yielding the topology shown in Fig. 3.

An inspection of this topology indicates two main regions where the connectivity constraint operates, both are circled in Fig. 3. The two regions have a width of roughly 3.7 mm, which is around the imposed minimum length A_{\min} of 4 mm. For further investigation, the activation parameter presented in Eq. (15) is plotted in Fig. 4.

The contrast between high and low values of the activation parameter illustrates the functionality of this process. The parameter maintains the connectivity where necessary without compromising the rest of the domain.

To evaluate the performance of the obtained structure, the dynamic response to a sinusoidal 1 kN excitation is calculated and shown in Fig. 5. Both the force and measurement points are placed vertically at the free end. The excitation frequency is swepted from 0 to 900 Hz.

The separation interval between the two natural frequencies around f_0 is increased by 28%, passing from 611.3 Hz to 785.4 Hz. Furthermore, the optimized structure is 60% lighter than the initial one.

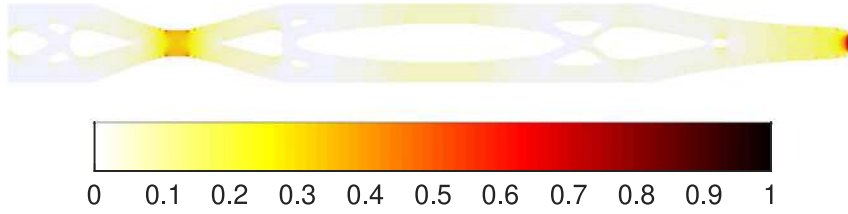


Fig. 4. Activation parameter on the final topology.

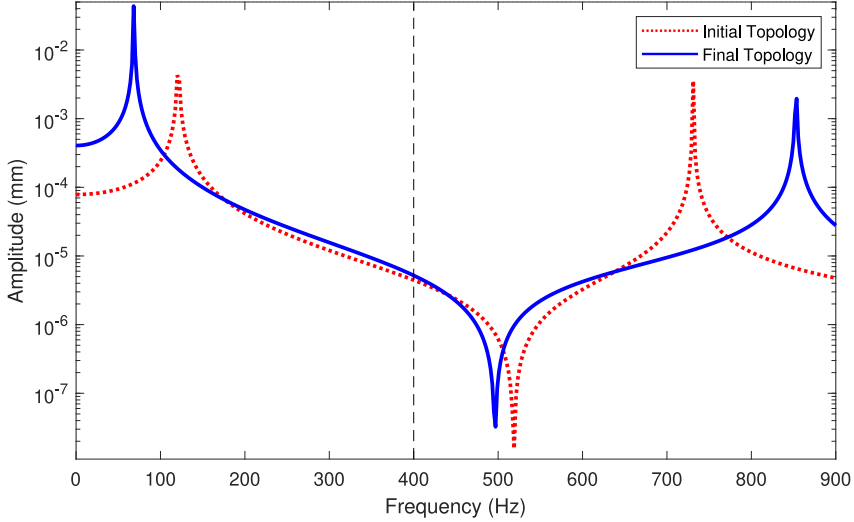


Fig. 5. Optimal topology frequency response.



Fig. 6. Optimal topology without connectivity constraint.

3.2. Optimization with design domain constraints

The results obtained in the previous section show the effectiveness of the proposed procedures. However, we aim at validating the proposed procedures experimentally. To realize the experiments under the same conditions, the displacements should be measured along the same external surface. Consequently, an exterior frame of 2 mm thickness is defined, and the optimization procedures should concern only the inner volume.

Additionally, a manufacturing constraint of a minimum thickness of 1.5 mm is considered. This is implemented by changing the sensitivity filter parameter r_{\min} to 1.5 mm. All other parameters are kept unchanged from the preliminary result.

Initially, the topology optimization procedure is performed without the connectivity procedure. Fig. 6 shows the optimized topology.

This topology is not a feasible solution. This structure would be both challenging to manufacture and could also present structural problems during experimentation.

This indicates that, despite the imposed fixed 2 mm layer, the connectivity procedure is necessary to obtain a proper solution. The input surface of the connectivity procedure is maintained as the left end, however, due to the fixed layer constraint, the output one is changed to the entire right extremity. The minimum connectivity width A_{\min} is also changed to 1.5 mm. Fig. 7 presents the obtained optimized structure.

Much like the preliminary analysis, the connectivity coefficient of each element is calculated and shown in Fig. 8.

While the values of the coefficient are not as high as those previously noted, they still pose an important effect on the procedure. The three most significant regions are shown in Fig. 8. A consequence of this procedure is that, although not strictly necessary to maintain connectivity in this case, it guarantees the minimum thickness required by the design constraints.

The evolution of the two first natural frequencies is shown in Fig. 9.



Fig. 7. Optimal topology with design constraints.

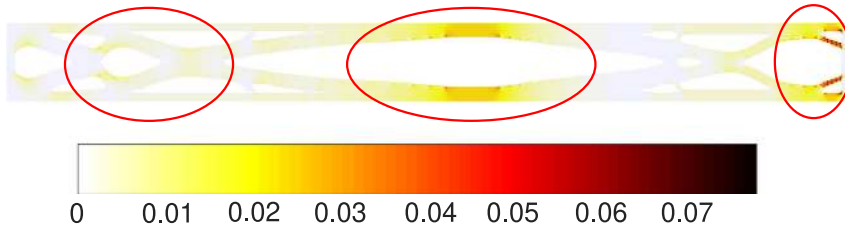


Fig. 8. Activation parameter on the final topology with design constraints.

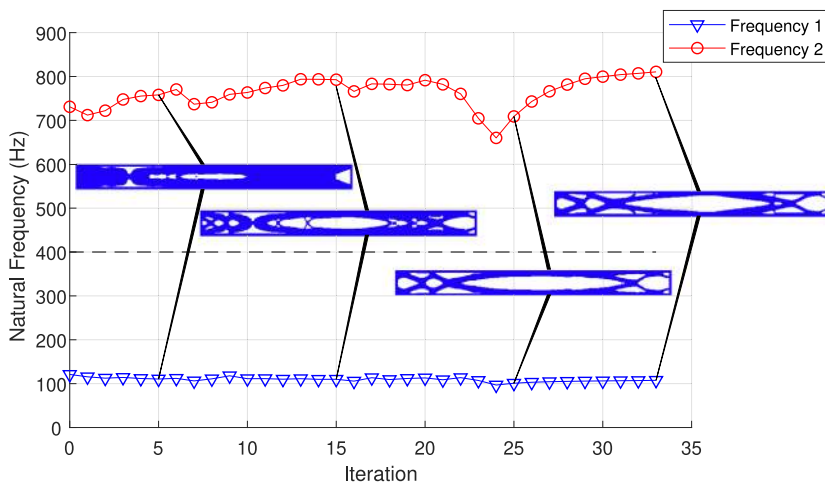


Fig. 9. Evolution of the first two natural frequencies with intermediary topologies.

It is observed that the first natural frequency varies little, while the second one changes more. From the beginning, the connectivity procedure maintains the connection near the base of the topology. Around iteration 25, a large decrease on the second natural frequency is observed due to the removal of internal bars. However, the procedure manages to increase it again by reinforcing other regions of the topology.

The natural frequency separation interval is visualized in Fig. 10.

The separation interval changes from 610 Hz to 703 Hz, totaling a 15% increase. This topology presents a satisfactory trade-off between design constraints and performance. Therefore, this result is chosen to proceed to the following analyses.

4. Three dimensional model

The three dimensional models are generated by extruding the two dimensional structures along the Z axis by a thickness of $t = 20$ mm. It is worth mentioning that this thickness was the suitable one following several simulations with different thicknesses.

Topology optimization procedures are applied during the preliminary design stage of an engineering project. Thus, the optimized topologies obtained from it are still subjected to alterations that aim at specific goals, such as guaranteeing manufacturability. Usually, smoothing techniques are employed to this end, enlarging or removing small features to ensure that the desired manufacturing process can produce it. In this work, two changes are implemented. First, sharp edges are smoothed, and internal bars are adjusted to guarantee a minimum thickness of 1.5 mm, ensuring the manufacturability of the specimens. Additionally, a rectangular base is added at the fixed end as an extension to the clamping device.

The Ansys® Workbench 17.0 software is employed to simulate the system and to generate the appropriate STL files for the 3D printer. The resulting model for the optimized structure is shown in Fig. 11.

A model for the initial structure is generated via a similar procedure. The FRFs of both structures are compared in Fig. 12.

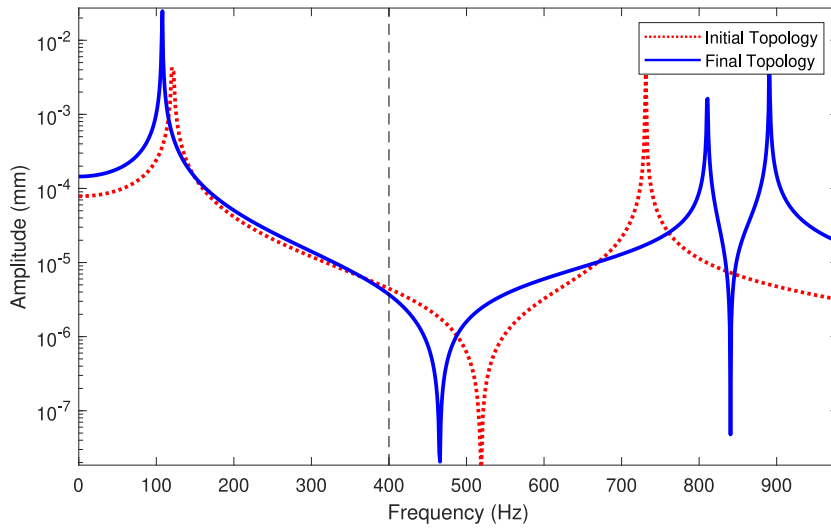


Fig. 10. Frequency response of optimal topology with design constraints.

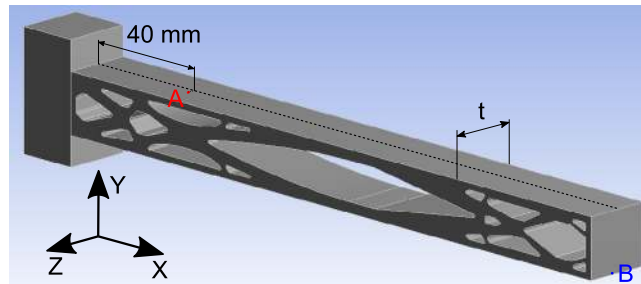


Fig. 11. Three-dimensional model of the optimized structure. A and B represent the points of force application and displacement measurement, respectively.

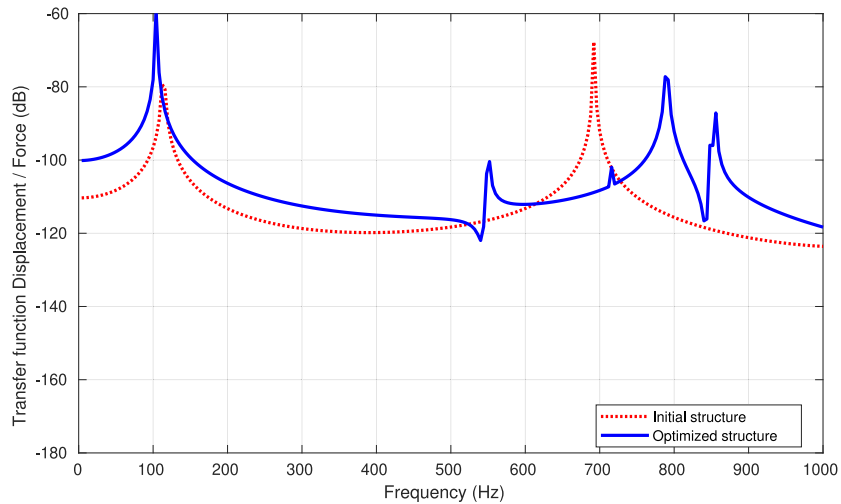


Fig. 12. Simulated FRFs from 3D initial and optimized structures.

Comparing the response of the three dimensional optimized structure to its two dimensional model counterpart, no significant difference is seen for the first resonance, around 104.5 Hz. The two resonances at 789.2 Hz and 850.2 Hz are also seen on the two dimensional model, although their values change slightly. Moreover, two new peaks are observed at 551.1 Hz and 716 Hz.

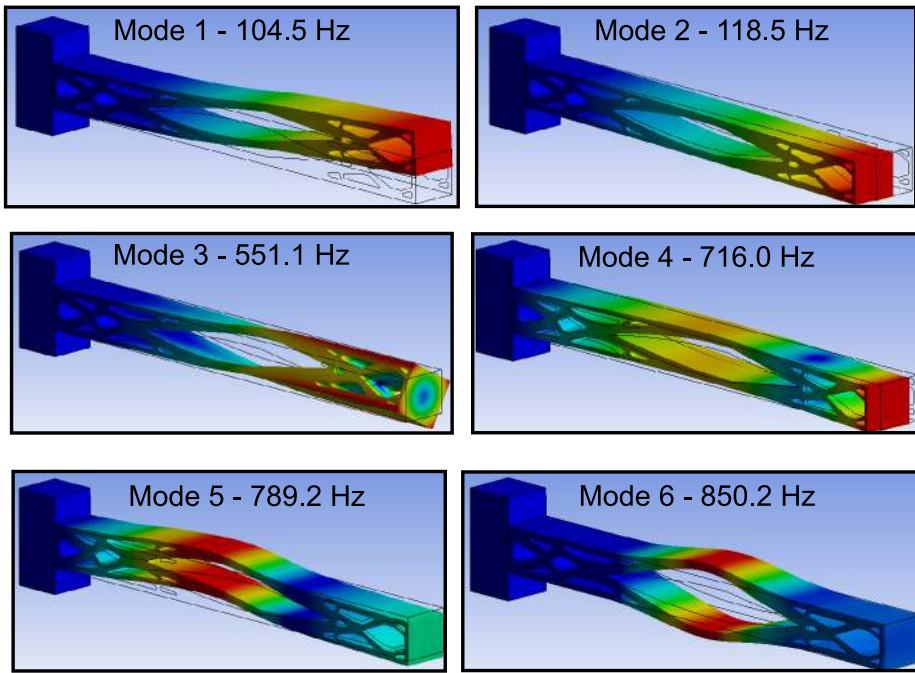


Fig. 13. Mode shape for the simulated model.

To study these new peaks, the eigenvalues and eigenvectors of the optimized topology are calculated. The mode shapes are shown in Fig. 13, along with their corresponding natural frequencies.

Modes 1, 5 and 6 are those that were optimized by the two dimensional topology optimization procedure and that were seen in both FRFs. Modes 2, 3 and 4, on the other hand, are the modes exclusive to the three dimensional analysis. Modes 2 and 4 correspond to the first and second bending modes in the $X-Z$ plane and Mode 3 is the first torsional mode. During the experimental analysis, as long as the force is as centered and as aligned to the Z direction as possible, these modes will be only slightly excited, so they are expected to exert little influence.

Having obtained a topology that satisfies the desired criteria, the experimental analysis can begin.

5. Experimental analysis

The experimental conditions and procedures will be presented first, then we will discuss the results obtained.

5.1. Experimental procedure

To manufacture the samples, a Lulzbot® Taz 6 printer was used. The specimens were built using a layer resolution of 0.1 mm, the printing direction was set parallel to the length of the structures (X axis), thereby the mechanical properties would be as close to the nominal ones as possible in this direction. The two manufactured structures are shown in Fig. 14.

The structures were clamped at one end and excited by using an electromagnetic shaker 40 mm from this clamped edge (Fig. 15). A force transducer placed between the push-rod and the structure enabled the measurement of the applied force. Decoupling the effects of the clamping support and the shaker from the dynamic behavior of the structure was a hard operation due to the small dimensions and mass of the samples. The shaker was suspended by elastic links, supervising that its influence would not affect the studied frequency range.

The laser vibrometer was set to sweep through several points on the structure surface to measure their velocity. It was placed 1.5 m from the surface of the sample, and its lens was aligned at 50 mm from the clamped end. White noise signal from 0 to 2000 Hz was used. It covered the studied frequency range and enabled easy and rapid measurements.

The measurement points were chosen in a distribution with a 13×5 grid along the surface of the structure (Fig. 16). The vibrometer was commanded and controlled via a software provided by the manufacturer. The sampling frequency was 2.5 kHz. The velocities and the force were measured and processed through 10 repetitions for each assessed point. The final responses were obtained by averaging each measurement. The list of equipment is shown in Table 2.

A general view of the setup and the equipment used is shown in Fig. 16.

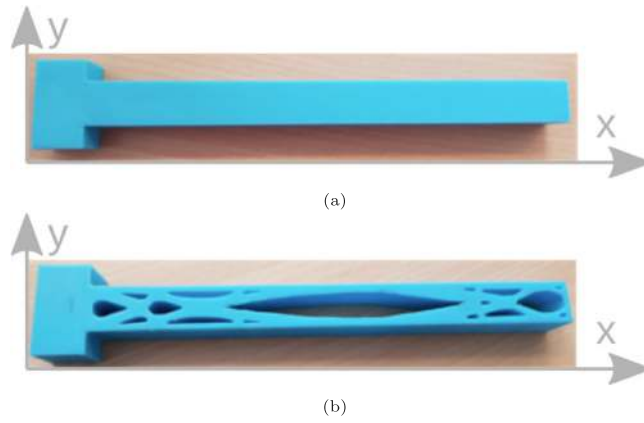


Fig. 14. Initial (a) and optimized (b) structures.

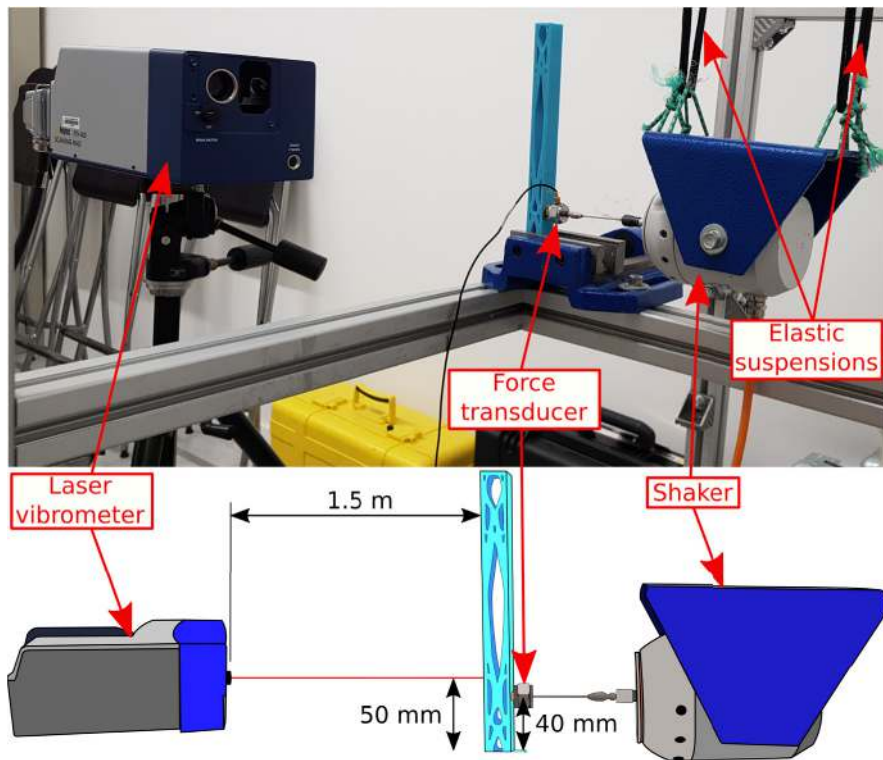


Fig. 15. Representation of the experimental setup.

Table 2
List of equipment.

Equipment	Model
Laser Doppler vibrometer	Polytec PSV-400
Force shaker	TIRA Vibration Exciter S 50018
Power amplifier	TIRA Power Amplifier BAA 60
Force transducer	Bruel & Kjaer Type 8200
Signal conditioner	Nexus Charge Conditioning Amplifier 2692-A

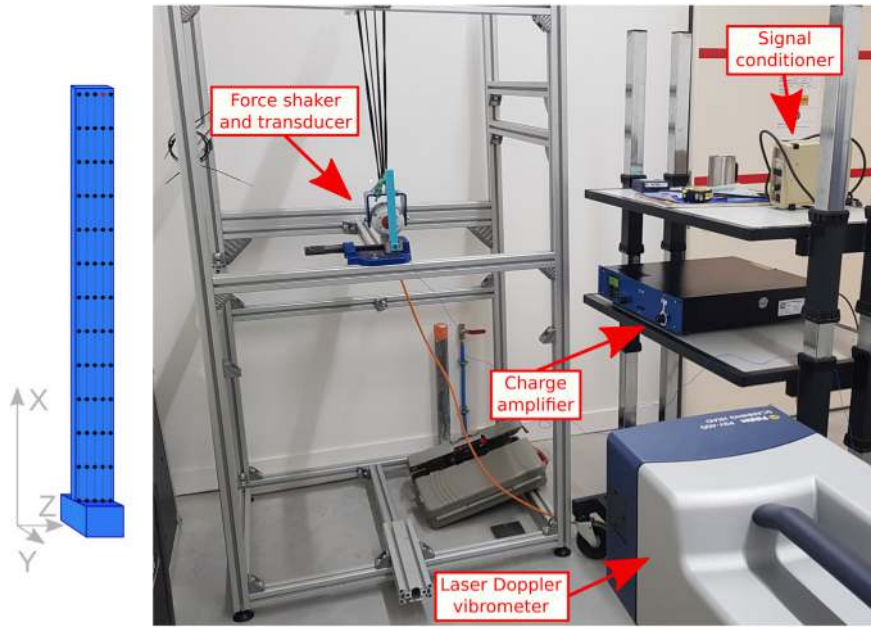


Fig. 16. General view of the experimental setup.

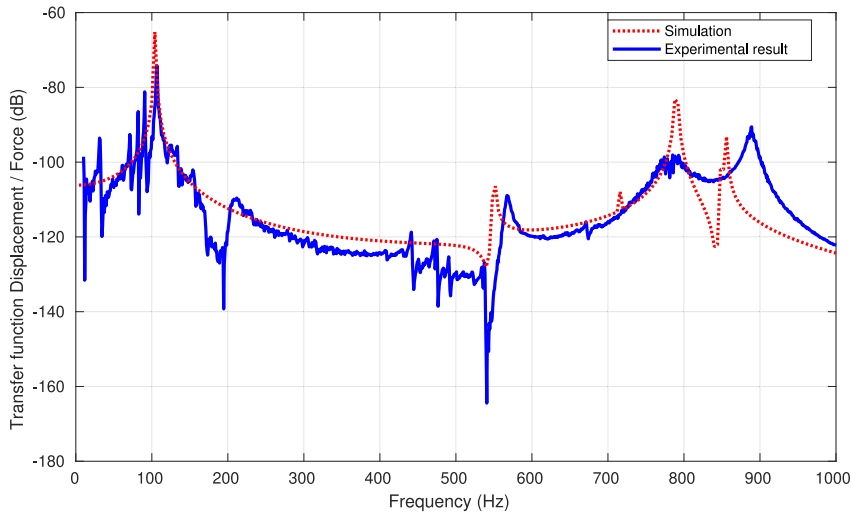


Fig. 17. Comparison between experimental and simulated FRFs, optimized structure.

5.2. Results and analysis

The post-treatment of the measured responses and the excitation enabled the representation of the FRFs, identifying the resonances and the corresponding mode shapes. The comparison between simulation and experimental FRFs is shown in Fig. 17.

For low frequency, due to the flexibility of the test rig and the shaker flexible suspensions, several peaks appeared. However, those suspension modes were low and were outside the studied frequency range.

The experimental response had a more complex dynamic behavior and several modes that had not been observed in the numerical simulations appeared. Those modes were due to the environment of the experiment. Numerical and measured resonance frequencies, for the considered frequency range, were similar as shown in Table 3.

The mode shapes of the identified resonances are shown in Fig. 18.

Comparing the experimental mode shapes with the numerical ones (Fig. 13), shows a good agreement. The modes in the orthogonal plan cannot be clearly seen in the experimentation. This is due to the capacity of the vibrometer. The fact that the

Table 3
First two bending frequencies (Hz).

Numerical simulation	Experiment	Difference
104.5	107.0	2.4%
789.2	790.0	0.1%

Table 4
First two bending frequencies (Hz).

	Resonance 1	Resonance 2	Difference
Initial structure	110.2	660.2	550.0
Optimized structure	107.0	790.0	683.0
Frequency separation interval increase			133.0

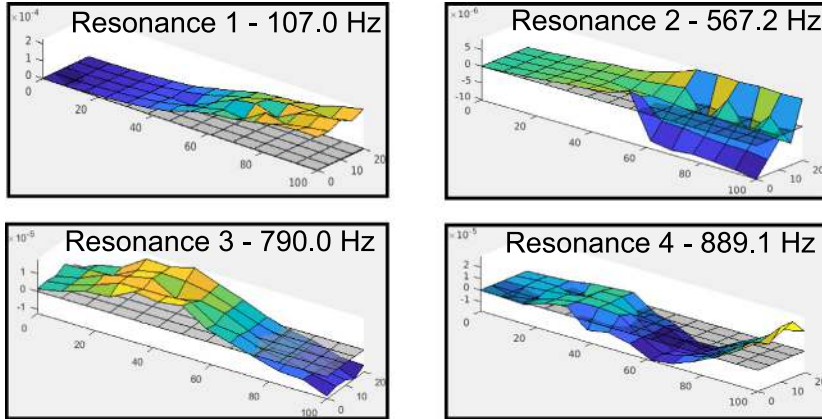


Fig. 18. Mode shape of the studied frequencies.

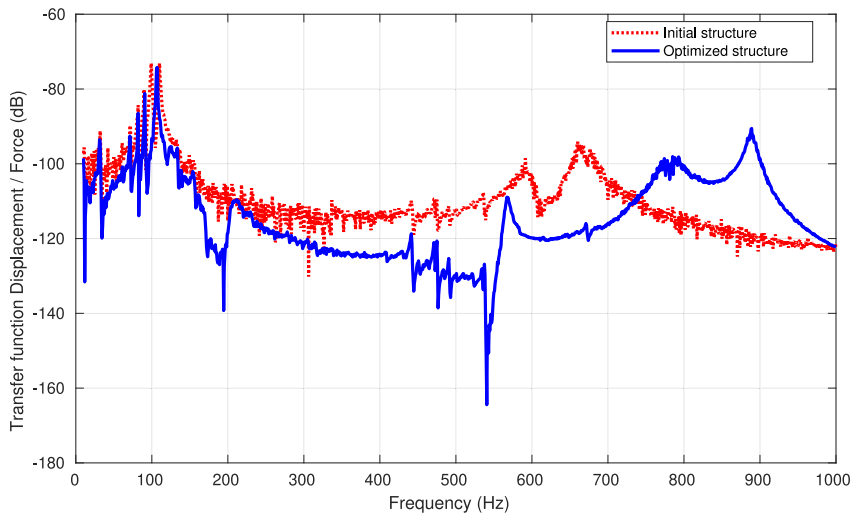


Fig. 19. FRFs of the optimized and the initial structures.

predicted behavior of the optimized structure matches correctly the measured one is important for the development of further studies on more complex structures.

Finally, the measured responses from both initial and optimized structures were compared experimentally, as illustrated in Fig. 19.

The first two bending frequencies of the initial and optimized structures are shown in Table 4.

The method produced a clear improvement of the dynamic response at the desired frequency range, as the frequency separation interval increased by 24%. Additionally, the optimized structure has a mass 40% lower than the initial one, decreasing from 108.0 g to 64.8 g.

The developed methodology enabled an increase of the frequency separation interval. The vibration levels, for almost all resonances in the studied frequency range decreased. Furthermore, the optimized topology had the desired behavior with a lower mass, which is of interest from a cost and an environmental points of view.

6. Conclusion

In this work, the design of an optimized elongated structure was performed. The optimization was done via the BESO method and was based on natural frequency separation criterion. The multi-domain topology optimization technique was employed to consider certain restrictions due to the manufacturing constraints. Also, a connectivity procedure based on the energy balance of an auxiliary problem was proposed to avoid non-physical solutions and to maintain certain geometric constraints.

The topology optimization analyses were performed on 2D structure. A 3D model was then generated by extruding the optimized 2D structures, considering several constraints in order to obtain a feasible topology for the experimental analysis. Numerical simulations were performed to compare the dynamic behavior of the initial and the optimized structure. An increase of 24% on the separation interval was obtained. Additional modes were observed in the analyzed frequency range for the optimized structure. This was expected when passing from 2D to 3D analysis.

Several prototypes were manufactured for the experimental analysis. The same trends were observed, few differences were noted due to the boundary conditions but they did not modify the obtained conclusions. The structure was excited by an electromagnetic shaker placed near the clamped end. In order to obtain the modal shapes for the studied frequency range, the displacements were measured using a laser Doppler vibrometer, along a grid of 5×13 points uniformly distributed.

Then, numerical predictions and experimental results were compared. The model describes the studied phenomena satisfactorily. The experimental response had a more complex dynamic behavior and several modes that were not observed in the numerical simulations appeared. Those modes were due to the environment of the experiment that could not be considered in the numerical simulations. This step was important in order to validate the proposed optimization strategy for further studies.

Finally, the measured dynamic responses of the initial and optimized structures were compared, and the frequency separation range increased by 133 Hz. Also, the vibration levels for almost all the observed modes decreased. The mass of the system was reduced by 40%.

The optimization algorithm can be readily applied for more complex structures. Further investigations must be conducted for more complete design problems. For example, techniques to couple dynamic and static requirements, such as stress constraints. Moreover, additional studies must be made on the BESO method and on the connectivity procedure to improve their robustness at producing feasible final topologies.

CRedit authorship contribution statement

Heitor Nigro Lopes: Conceptualization, Methodology, Software, Investigation, Writing – original draft. **Daniel Candeloro Cunha:** Conceptualization, Methodology, Formal analysis, Writing – review & editing. **Renato Pavanello:** Conceptualization, Writing – review & editing, Supervision, Project administration, Funding acquisition. **Jarir Mahfoud:** Investigation, Resources, Writing – review & editing, Funding acquisition.

Declaration of competing interest

The authors declare that they have no known competing financial interests or personal relationships that could have appeared to influence the work reported in this paper.

Acknowledgments

This work was supported by FAPESP (São Paulo Research Foundation, grant numbers 2013/08293-7, 2019/19237-7 and 2019/05393-7) and CNPq (National Council for Scientific and Technological Development, grant number 130636/2019-3).

References

- [1] S. Zargham, T.A. Ward, R. Ramli, I.A. Badruddin, Topology optimization: A review for structural designs under vibration problems, *Struct. Multidiscip. Optim.* 53 (6) (2016) 1157–1177, <http://dx.doi.org/10.1007/s00158-015-1370-5>.
- [2] M.P. Bendsoe, N. Kikuchi, Generating optimal topologies in structural design using a homogenization method, *Comput. Methods Appl. Mech. Engrg.* 71 (2) (1988) 197–224, [http://dx.doi.org/10.1016/0045-7825\(88\)90086-2](http://dx.doi.org/10.1016/0045-7825(88)90086-2).
- [3] M. Bendsoe, Optimal shape design as a material distribution problem, *Struct. Optim.* (1989) 10.
- [4] M. Zhou, G. Rozvany, The COC algorithm, part II: topological, geometrical and generalized shape optimization, *Comput. Methods Appl. Mech. Engrg.* 89 (1–3) (1991) 309–336, [http://dx.doi.org/10.1016/0045-7825\(91\)90046-9](http://dx.doi.org/10.1016/0045-7825(91)90046-9).
- [5] G. Rozvany, M. Zhou, T. Birker, Generalized shape optimization without homogenization, *Struct. Optim.* 4 (3–4) (1992) 250–252, <http://dx.doi.org/10.1007/BF01742754>.

- [6] Y. Xie, G. Steven, A simple evolutionary procedure for structural optimization, *Comput. Struct.* 49 (5) (1993) 885–896, [http://dx.doi.org/10.1016/0045-7949\(93\)90035-C](http://dx.doi.org/10.1016/0045-7949(93)90035-C).
- [7] O. Querin, G. Steven, Y. Xie, Evolutionary structural optimisation (ESO) using a bidirectional algorithm, *Eng. Comput.* 15 (8) (1998) 1031–1048, <http://dx.doi.org/10.1108/02644409810244129>.
- [8] A. Díaz, O. Sigmund, Checkerboard patterns in layout optimization, *Struct. Optim.* 10 (1) (1995) 40–45, <http://dx.doi.org/10.1007/BF01743693>.
- [9] X. Huang, Y. Xie, Convergent and mesh-independent solutions for the bi-directional evolutionary structural optimization method, *Finite Elem. Anal. Des.* 43 (14) (2007) 1039–1049, <http://dx.doi.org/10.1016/j.finel.2007.06.006>.
- [10] N. Pedersen, Maximization of eigenvalues using topology optimization, *Struct. Multidiscip. Optim.* 20 (1) (2000) 2–11, <http://dx.doi.org/10.1007/s001580050130>.
- [11] X. Huang, Z. Zuo, Y. Xie, Evolutionary topological optimization of vibrating continuum structures for natural frequencies, *Comput. Struct.* 88 (5–6) (2010) 357–364, <http://dx.doi.org/10.1016/j.compstruc.2009.11.011>.
- [12] R. Picelli, W. Vicente, R. Pavanello, Y. Xie, Evolutionary topology optimization for natural frequency maximization problems considering acoustic–structure interaction, *Finite Elem. Anal. Des.* 106 (2015) 56–64, <http://dx.doi.org/10.1016/j.finel.2015.07.010>.
- [13] W. Vicente, R. Picelli, R. Pavanello, Y. Xie, Topology optimization of frequency responses of fluid–structure interaction systems, *Finite Elem. Anal. Des.* 98 (2015) 1–13, <http://dx.doi.org/10.1016/j.finel.2015.01.009>.
- [14] N. Chen, S. Xia, J. Liu, Z. Ma, Microstructural topology optimization for minimizing the sound pressure level of structural-acoustic systems with multi-scale bounded hybrid uncertain parameters, *Mech. Syst. Signal Process.* 134 (2019) 106336, <http://dx.doi.org/10.1016/j.ymssp.2019.106336>.
- [15] Y. Zhang, M. Xiao, L. Gao, J. Gao, H. Li, Multiscale topology optimization for minimizing frequency responses of cellular composites with connectable graded microstructures, *Mech. Syst. Signal Process.* 135 (2020) 106369, <http://dx.doi.org/10.1016/j.ymssp.2019.106369>.
- [16] B.V. de Almeida, D.C. Cunha, R. Pavanello, Topology optimization of bimorph piezoelectric energy harvesters considering variable electrode location, *Smart Mater. Struct.* 28 (8) (2019) 085030, <http://dx.doi.org/10.1088/1361-665X/ab2c3e>.
- [17] Y. Chen, F. Meng, X. Huang, Creating acoustic topological insulators through topology optimization, *Mech. Syst. Signal Process.* 146 (2021) 107054, <http://dx.doi.org/10.1016/j.ymssp.2020.107054>.
- [18] Z.-Q. Lin, H.C. Gea, S.-T. Liu, Design of piezoelectric energy harvesting devices subjected to broadband random vibrations by applying topology optimization, *Acta Mech. Sinica* 27 (5) (2011) 730–737, <http://dx.doi.org/10.1007/s10409-011-0491-3>.
- [19] C. Sultan, Designing structures for dynamical properties via natural frequencies separation, *Mech. Syst. Signal Process.* 23 (4) (2009) 1112–1122, <http://dx.doi.org/10.1016/j.ymssp.2008.08.014>.
- [20] Z.D. Ma, N. Kikuchi, I. Hagiwara, Structural topology and shape optimization for a frequency response problem, *Comput. Mech.* 13 (3) (1993) 157–174, <http://dx.doi.org/10.1007/BF00370133>.
- [21] Z.-D. Ma, H.-C. Cheng, N. Kikuchi, Structural design for obtaining desired eigenfrequencies by using the topology and shape optimization method, *Comput. Syst. Eng.* 5 (1) (1994) 77–89, [http://dx.doi.org/10.1016/0956-0521\(94\)90039-6](http://dx.doi.org/10.1016/0956-0521(94)90039-6).
- [22] Y. Xie, G. Steven, A simple approach to structural frequency optimization, *Comput. Struct.* 53 (6) (1994) 1487–1491, [http://dx.doi.org/10.1016/0045-7949\(94\)90414-6](http://dx.doi.org/10.1016/0045-7949(94)90414-6).
- [23] J.S. Jensen, N.L. Pedersen, On maximal eigenfrequency separation in two-material structures: The 1D and 2D scalar cases, *J. Sound Vib.* 289 (4–5) (2006) 967–986, <http://dx.doi.org/10.1016/j.jsv.2005.03.028>.
- [24] J. Du, N. Olhoff, Topological design of freely vibrating continuum structures for maximum values of simple and multiple eigenfrequencies and frequency gaps, *Struct. Multidiscip. Optim.* 34 (2) (2007) 91–110, <http://dx.doi.org/10.1007/s00158-007-0101-y>.
- [25] Z. Li, T. Shi, Q. Xia, Eliminate localized eigenmodes in level set based topology optimization for the maximization of the first eigenfrequency of vibration, *Adv. Eng. Softw.* 107 (2017) 59–70, <http://dx.doi.org/10.1016/j.advengsoft.2016.12.001>.
- [26] Q. Li, Q. Wu, J. Liu, J. He, S. Liu, Topology optimization of vibrating structures with frequency band constraints, *Struct. Multidiscip. Optim.* (2020) <http://dx.doi.org/10.1007/s00158-020-02753-7>.
- [27] H.N. Lopes, J. Mahfoud, R. Pavanello, High natural frequency gap topology optimization of bi-material elastic structures and band gap analysis, *Struct. Multidiscip. Optim.* (2021) <http://dx.doi.org/10.1007/s00158-020-02811-0>.
- [28] S. Adhikari, Damping modelling using generalized proportional damping, *J. Sound Vib.* 293 (1–2) (2006) 156–170, <http://dx.doi.org/10.1016/j.jsv.2005.09.034>.
- [29] Q. Liu, D. Ruan, X. Huang, Topology optimization of viscoelastic materials on damping and frequency of macrostructures, *Comput. Methods Appl. Mech. Engrg.* 337 (2018) 305–323, <http://dx.doi.org/10.1016/j.cma.2018.03.044>.
- [30] C. Sultan, Proportional damping approximation using the energy gain and simultaneous perturbation stochastic approximation, *Mech. Syst. Signal Process.* 24 (7) (2010) 2210–2224, <http://dx.doi.org/10.1016/j.ymssp.2010.02.013>.
- [31] Z.-D. Ma, H. Wang, N. Kikuchi, C. Pierre, B. Raju, Experimental validation and prototyping of optimum designs obtained from topology optimization, *Struct. Multidiscip. Optim.* 31 (5) (2006) 333–343, <http://dx.doi.org/10.1007/s00158-005-0530-4>.
- [32] C. Zhao, G. Steven, Y. Xie, Evolutionary natural frequency optimization of two-dimensional structures with additional non-structural lumped masses, *Eng. Comput.* 14 (2) (1997) 233–251, <http://dx.doi.org/10.1108/02644409710166208>.
- [33] Z. Zuo, Y. Xie, X. Huang, An improved bi-directional evolutionary topology optimization method for frequencies, *Int. J. Struct. Stab. Dyn.* 10 (01) (2010) 55–75, <http://dx.doi.org/10.1142/S0219455410003415>.
- [34] D.J. Munk, G.A. Vio, G.P. Steven, A bi-directional evolutionary structural optimisation algorithm with an added connectivity constraint, *Finite Elem. Anal. Des.* 131 (2017) 25–42, <http://dx.doi.org/10.1016/j.finel.2017.03.005>.
- [35] S. Liu, Q. Li, W. Chen, L. Tong, G. Cheng, An identification method for enclosed voids restriction in manufacturability design for additive manufacturing structures, *Front. Mech. Eng.* 10 (2) (2015) 126–137, <http://dx.doi.org/10.1007/s11465-015-0340-3>.
- [36] Y. Luo, O. Sigmund, Q. Li, S. Liu, Additive manufacturing oriented topology optimization of structures with self-supported enclosed voids, *Comput. Methods Appl. Mech. Engrg.* 372 (2020) 113385, <http://dx.doi.org/10.1016/j.cma.2020.113385>.
- [37] Z. Hashin, S. Shtrikman, A variational approach to the theory of the elastic behaviour of multiphase materials, *J. Mech. Phys. Solids* 11 (2) (1963) 127–140, [http://dx.doi.org/10.1016/0022-5096\(63\)90060-7](http://dx.doi.org/10.1016/0022-5096(63)90060-7).